The Impact of Snow Conditions in Spring Dynamical Seasonal Predictions

C. Adam Schlosser

Goddard Earth Science and Technology Center

Hydrological Sciences Branch

NASA Goddard Space Flight Center

and

David M. Mocko

Climate and Radiation Branch

Laboratory for Atmospheres

NASA Goddard Space Flight Center

Additional affiliation: SAIC/General Sciences Operation

Submitted to the GCIP Issue of

Journal of Geophysical Research - Atmospheres

January 9, 2003

Abstract

A suite of numerical simulations with the Center for Ocean Land Atmosphere (COLA) Studies' and the Goddard Earth Observing System (GEOS) general circulation models (GCMs) has been performed in conjunction with the Dynamical Seasonal Prediction (DSP) Project. These simulations aim to quantify the impact of realistic snow conditions on skill in the GCMs. In this study, ensemble climate simulations conducted for Northern Hemisphere spring (March-June) that span the years 1982-1998 are considered. For each year of these seasonal simulations, a pair of complementary runs is performed. For one of the simulations, snow conditions are allowed to evolve interactively; for the other simulation, the snow conditions are prescribed - according to a daily, global snow depth analysis - within each of the land modules of the GCMs. For this study, the impact of snow conditions on simulated near-surface air temperature is assessed.

The results indicate that the prescribed (and presumably improved) snow conditions in the GCMs play a beneficial role toward skillfully capturing the observed spatial/temporal patterns of interannual variations of near-surface air temperature - at a local scale. Through consideration of the surface energy-budget and the effect of snow cover on surface albedo, the localized improvement of near-surface air temperature skill (both in the spatial correlations and root-mean square error) that results from the prescribed snow fields is found to be strongly tied to when and where the interannual variability of snow cover and mean incident short wave radiation coincide. This impact of prescribed snow is also most considerable during the widespread ablation of the matured winter-season

snow cover, which typically occurs during April over the Northern Hemisphere. Overall, the impact of the prescribed snow over all land points (i.e. local and non-local) shows mixed results in its effect on near-surface air temperature skill. These mixed results most likely underscore the difficulty of the GCMs to consistently translate the localized skillful response into non-local/remote skill. In the end, physical parameterizations in GCMs should be improved before all seasonal prediction enhancements from improved snow conditions can be realized.

1. Introduction

Research into the determination of the extent that snow variations play an active role in large-scale climate oscillations is considerable. For example, numerous studies have investigated the relationship of winter Eurasian snow cover and the following season Indian monsoon or Eurasian rainfall (*e.g.*, Vernekar *et al.*, 1995; Bamzai and Shukla, 1999). Observational data of snow cover and temperature has also shown that the snow cover strongly modifies the local air temperature for a period of days to a season (Foster *et al.*, 1983; Namias, 1985). One of the primary effects of the presence snow cover has been demonstrated to be on surface albedo, which reduces the shortwave radiation absorbed at the ground, and thus the surface temperature (*e.g.*, Groisman *et al.*, 1994). Walsh and Ross (1988) showed using a global circulation model (GCM) that years with heavy snow cover had a reduction in surface air temperature in the area of the snow anomaly. Cohen and Rind (1991), however, showed in a GCM that the snow effect on temperature was short term, as a result of secondary effects of modifications to sensible and latent heat fluxes and emitted longwave radiation. On the other hand, Yang *et al.* (2001) showed with a GCM that the local snow albedo feedback strongly enhances the surface air temperature anomalies over North America for El Niño minus La Niña years.

Simulations of snow in various GCMs (*e.g.*, Foster *et al.*, 1996) and land models (*e.g.*, Schlosser *et al.*, 2000; Slater *et al.*, 2001) as compared to in-situ observations and remotely sensed datasets show that models have difficulties simulating snow cover and depths during transition months of the spring and fall, as well as mid-season ablation

events. These errors in snow cover can then produce subsequent errors in the local temperatures and soil moisture, and could adversely affect precipitation (in a coupled model framework). One method of reducing these errors is assimilation of snow depth data during model integration. Through the application of a coherent observation operator to assimilate snow depth, Urban (1996) was able to obtain an improvement in the simulation of surface air temperature in 16-day assimilation run with a GCM. While the Urban (1996) result is limited to the meteorological condition considered (initialization of assimilation run: December 12, 1994), the result indicates the potential effect of improved snow conditions in climate models, and warrants the extension of these types of prescribed snow experiments in GCMs to assess impacts over longer integrations (*i.e.*, months to seasons) and over a variety of climate conditions (*i.e.*, multiple years/decades of seasonal integrations).

To that end, this study explores the impact of snow conditions on the skill of seasonal climate simulations for two general circulation models (GCMs): The Center for Ocean Land Atmosphere (COLA) and the Goddard Earth Observing System (GEOS). Experimental seasonal simulations (*i.e.*, March-June) are conducted for the years 1982-1998 using interactive and prescribed snow conditions. The prescribed snow conditions are based on a global, daily snow analysis that is compiled by the US Air Force (described in the section 2). Using station observations of near-surface air temperature, the impact of the prescribed snow conditions on the GCMs' performance is then assessed. In the next section, the GCMs employed, the global snow depth analysis used, and the numerical experiments conducted are described. The results of the numerical

experiments and an assessment of the prescribed snow's impacts are discussed in Section 3. Discussion and concluding remarks are given in Section 4.

2. Models, Snow Data and Numerical Experiments

a. Models

One of the GCMs used in this study is the Goddard Earth Observing System (GEOS) general circulation model (Conaty *et al.*, 2001). The GEOS GCM is primarily used for climate studies and data assimilation at the Goddard Laboratory for Atmospheres. The hydrodynamics of the model are on a C-grid (Takacs *et al.*, 1994). The boundary-layer scheme for turbulent transport is by Helfand and Lebraga (1988), and the gravity-wave drag parameterization of Zhou *et al.* (1996) is included. Recently, the GEOS GCM has included major improvements to its physical processes such as its convective parameterization, radiation, and land-surface representation. The convective parameterization used is the Microphysics of clouds with Relaxed Arakawa-Schubert scheme (McRAS, Sud and Walker, 1999a&b). The radiation package used for this study is due to Chou and Suarez (1994), and Chou *et al.* (1998 & 1999). The land-surface model is the HY-SSiB model, which is based on the Simplified Simple Biosphere Model (SSiB) from Xue *et al.* (1991), but includes upgrades to its snow physics and hydrology (Sud and Mocko, 1999; Mocko and Sud, 2001). The snow on the ground is represented by two layers - a bulk snow layer and a thin "diurnal" snow depth at the top of the snowpack. These two layers evolve via their individual energy budget and heat exchange

between them as well as the ground below. The top snow layer is responsive to the atmosphere's diurnal cycle, which can produce midday and midwinter snow melting. Downward shortwave energy can be reflected by the snow, absorbed within the snowpack, or transmitted through the snow to the ground. Liquid water in the snowpack is calculated, and an age effect of the snow exists which increases the snow density with time.

The other atmospheric GCM (AGCM) used in this study is from the Center for Ocean Land Atmosphere (COLA), documented by Kinter et al. (1997). It is a research version of the global spectral model described by Sela (1980), and the most recent changes have been documented by Schneider (2002). The land surface is represented by a modified version of the simplified Simple Biosphere Model (SSiB; Xue *et al.*, 1991) that is described in Dirmeyer and Zeng (1999). In particular, the evolution of the snow pack in the COLA-SSiB model is represented by a water-equivalent snow depth and is tracked as a bulk, single-layer storage (analogous to the "bucket" model representation of soil-moisture storage). Increases in snowpack are a consequence of snowfall, and decreases in snow depth are a result of melting and sublimation. In addition, the effect of the snow pack on the surface energy budget is represented implicitly by: lumping the thermal heat capacity of the uppermost soil layer together with changes in the water-equivalent heat capacity of the snow pack; and modulations in the aggregate grid-box albedo (discussed further in Section 3b).

b. USAF snow depth estimates

This data set is a global daily snow depth product (1979-1998) that is used routinely by the United States Air Force (USAF) and is also the basis of the Eta operational weather forecasting system's snow initialization field (K. Mitchell, personal communication, 2002). It produces daily maps of snow depth and snow age for the northern and southern hemispheres, and the analysis is based on surface synoptic weather observations, snow climatology (Foster and Davey, 1988), time continuity and manual updates. The data are "gridded" to an eighth-mesh reference grid that divides each hemisphere into 64 x 64 cells. Each of these cells is further subdivided into 64 x 64 further cells with each one having an approximate dimension of 46.3 km x 46.3 km. For each of these cells, a snow depth value is assigned (to the nearest inch) which is based on snow depth observations from meteorological stations or user-estimated snow depth (based on snow climatology and time continuity) available within the 46.3 km x 46.3 km domain. A complete description of the data and its construction is described by Hall (1986). Recently, this data has been re-formatted by the Center for Ocean Land Atmosphere Studies for use in climate research (Fennessy and Schlosser, 2002). Figure 1 shows the averaged (1979-1998) 1st day of the month fields of snow depth for March-June (which fall within the period of the GCM seasonal integrations conducted, discussed in the next section).

In regions where the network of snow depth measurements at meteorological stations is sparse (Antarctica, Greenland and the Arctic, China, Mountainous terrain, ice-covered areas), different methodologies are used to estimate snow depth in these areas. For example, in Antarctica, snow depth is derived from an estimation of the snow water

equivalent and the density. These two parameters are estimated from precipitation and from observations of snow density variations around the continent. Compensation of snow depth around the coastal fringe is also applied to prevent overestimation in these areas (due to the presence of liquid precipitation). In Greenland and Antarctica and in mountainous terrain, a similar method is used. For China and ice covered areas, climate atlases are used to estimate snow depth. For several countries, qualitative confidence levels are provided ranging from high to low. These labels are described in Foster and Davey (1988) and were determined from literature documenting the data ingested into the synoptic data sets and are generalized confidence values for the entire country.

c. Model experiments

i) Control run – the Ocean Boundary Only Experiment (OBOE)

For both AGCMs, the experimental design follows that of the Dynamical Seasonal Prediction (DSP) project (Shukla *et al.*, 2000). As most of the land states are set to climatological values initially (described below), the major source of an anomalous boundary-forced response would be the prescribed SSTs. As such, we hereafter denote these simulations as the Ocean Boundary Only Experiment - or the "OBOE" simulations. For the COLA AGCM, ensembles of ten integrations at a spectral truncation of T63 (~1.875E grid resolution) were completed for 17 consecutive years for the period March-June (MAMJ). These simulations were run for the years 1982-1998. Five of the ensemble members are initialized from the 0000UTC National Center for Environmental

Prediction (NCEP) global reanalyses (Kalnay *et al.*, 1996) on the last five days of February. The other five members are initialized by perturbing the 0000UTC states based on extrapolation from the subsequent 1200UTC NCEP reanalyses. All of the initial land surface states (except snow) are climatological values from a 21-year off-line simulation with the same land-surface model (Dirmeyer and Tan, 2001). The initial snow cover is also a climatological value based on a land albedo data set (Posey and Clapp, 1954).

For the GEOS model, the same 17 years of 1982-1998 were simulated, but with only one member in the "ensemble". This was done, in part, due to constraints in computational allocations, and therefore the GEOS GCM's response to snow from a single realization of the atmosphere for all the years (1982-1998) would likely be more informative than multi-member ensembles for only a subset of years in the 1982-1998 period. The initial condition of the atmosphere for each year was interpolated from the 1 March ECMWF reanalysis of that year. The initial land surface states (except snow) were taken from 1 March 1987/1988 averaged values from a Global Soil Wetness Project (Dirmeyer *et al.*, 1999) style off-line simulation with the identical HY-SSiB land-surface model used in GEOS. The initial snow cover for each year was taken from the 1 March USAF snow depth estimates. The configuration of the GEOS GCM for this study was a grid spacing of 2 deg. latitude X 2.5 deg. longitude with 20 sigma-layers in the vertical.

ii) The Snow "ASsimilation" Experiment (SASE)

In these experimental simulations, the OBOE simulations are repeated, but with the USAF daily snow depth analysis inserted into the land module. The "assimilation" of snow in the GCMs for this study is not a rigorous assimilation of the data, but rather a "direct insertion" of the snow depth data. This direct insertion of the USAF snow data was performed daily (at 0Z) and globally during the course of the SASE simulations. For the time periods between subsequent 0Z prescriptions, the snow pack was allowed to evolve freely according to the land models' prognosis. In doing so, the USAF snow data is regarded as hypothetically "perfect information" of snow conditions, and thus no "assimilation" of the data (to account for errors in the observations) would be required. In addition, the USAF analysis is a snow depth product, and thus does not provide any information as to the density of snow (nor the water equivalent snow depth). Thus, in order to provide a value of snow water equivalent depth, which is the prognostic variable of snow in the COLA and GEOS land models, gross assumptions had to be made regarding snow density. While the density of a snow pack can vary considerably according to temperature, age, morphology, melt/re-freeze, rain on snow, etc. (*e.g.*, Warren, 1984), no such complementary daily, global mapping of these contributing effects on snow density exists. Therefore, a snow density value of 200 kg/m^3 (*i.e.*, a 5:1 ratio of snow depth to water-equivalent snow depth) was applied globally. While this value of snow density falls within the median range of recorded snow pack densities (*e.g.*, Doesken and Judson, 1997), the global assignment of this constant value (in space and time) is, certainly, crude. However, the intent of these simulations lies more in the assessment of the sensitivity of GCMs to more realistic snow conditions (prescribed by the USAF daily analysis) rather than to rigorously address the utility of the USAF snow

data for data assimilation. The subsequent analysis presented in the next section, and the interpretation and discussion of the results (section 4), will be addressed accordingly in light of the assumptions and simplifications made in constructing these Snow "ASsimilation" Experiment (SASE) simulations.

3. Results

In the analysis that follows, only land points between 20E N and 75E N are considered. In addition, the model diagnoses for April mean quantities are presented. This was done in light of the USAF analysis indicating that, typically, the most considerable retreat and ablation of the ephemeral (i.e. seasonal) snow cover occurs during the month of April and within the 20E N and 75E N latitude band (Fig. 1), and therefore the impact of the transition from snow cover to bare ground is typically at its maximum. Furthermore, in all the diagnostics provided below for the April mean quantities, generally speaking, the corresponding results for the March, May and June outputs show a weaker response.

a. Mean response to prescribed snow conditions

Given that both the COLA and GEOS GCMs contain differences in their simulated climatologies of snow cover, the prescribed snow conditions in the SASE experiments will likely induce different degrees and patterns of mean temperature response. For the COLA model, the most considerable change in the April snow cover patterns from the OBOE to SASE simulations is an overall increase snow coverage, with the largest

increases over most of eastern Canada, the Baltic region, and western Russia (Fig. 2). Slight decreases are imposed along the coast of western Canada. Due to the presence of increased snow coverage, a subsequent decrease in April T_a is seen (Fig. 3) particularly over the Baltic region and western Russia. For the GEOS model, an overall increase in snow cover results from the prescribed snow conditions (Fig. 4) – which is similar to the COLA GCM. However, unlike the COLA GCM, the most considerable increases in snow cover are found over central to eastern Russia and farther north in eastern Canada (and to a stronger degree). This results in substantially larger decreases in T_a (Fig. 5) as compared to the COLA model.

Subsequent changes in the interannual variability of snow cover and T_a were also seen. Generally speaking, a southerly shift in the relative maxima of snow cover variability is found in both of the GCMs' SASE simulations (Fig. 6). However, for the GEOS model, the southerly shift is accompanied by a decrease in the relative maximum values, whereas the COLA model shows very small changes in the relative extreme values. Correspondent with these shifts in the maximum variability of snow cover were changes in the patterns of T_a variability (not shown), in which the regions of increased snow cover variability in the SASE simulations also show an increase in T_a variability (and conversely so). Overall, the changes seen in the mean and variability of snow coverage and T_a in the COLA model's SASE simulations are improvements upon previously documented shortcomings (Schlosser and Dirmeyer, 2000). Proper snow cover simulation and soil moisture "assimilation" has also been shown to have beneficial effects on GEOS climate simulations (Mocko *et al.*, 1999; Sud *et al.*, 2002).

b. Impact of prescribed snow on simulated temperature anomalies

Simulated values of surface air temperature (T_a) from each of the two models for all simulation years were compared to the CAMS near-surface air temperature data (Ropelewski *et al.*, 1985). Figure 7 (top panel) shows the spatial correlation coefficient between the anomalies of monthly-averaged April values from the COLA simulations and the CAMS data as well as the same comparison between the GEOS simulations and the CAMS data (bottom panel). Neither model shows significant improvement in near-surface air temperature skill of the SASE simulations over the OBOE simulations. Several years do show some improvement, but a few other years show a slight degradation in skill. The two different models occasionally produced different results for the same year. For example, the COLA model shows a strong improvement in the SASE runs for 1990 and 1991, while the GEOS model SASE runs have little effect, whereas the GEOS model shows a strong improvement in 1982 and 1983, while the COLA model has only a small increase in skill. Furthermore, while some of the most considerable correlation increases are seen in ENSO years for the GEOS model, all of the considerable correlation increases occur in non-ENSO years for the COLA model (and no increases are seen in ENSO years). Similar, though less robust, results were found for the other months of these MAMJ simulations (not shown). Some similarities between the models do exist, however, such as the relatively good skill in the years 1987 and 1997, as well as the decrease in skill in the SASE runs of 1986 and 1994.

Not only are the patterns of temperature anomalies affected by the prescribed snow conditions, but also the mean error (Fig. 8 – results for same points as in Fig. 7). The RMS errors for the OBOE simulations are generally between 1.0 and 1.4 K, while the SASE runs for the most part reduce this error slightly, even to less then 1.0 K for some years. Again, some of the strongest improvements are in the COLA model for the year 1990 and 1991, and in the GEOS model for 1982 and 1983. The 1997 RMS error is not significantly less than the other years for either model despite attaining their highest spatial correlation of temperature anomalies (Fig. 7).

c. "Local" impacts of snow in the GCMs

The mixed results in simulated T_a skill scores (both the spatial correlation and RMS errors) for all the 20EN and 75EN land points in the COLA and GEOS GCMs indicate that the prescribed snow conditions did not ubiquitously (in space and time) result in more accurate temperature responses. Certainly, the overall skill sensitivities (Figs. 7 and 8) are a combination of "local" (within a grid-box) effects on the simulated atmosphere to the prescribed snow conditions, and non-local responses, which result from the simulated atmosphere's advection of the local snow impacts. To first order, a correction in snow cover should at least induce a localized improvement in the GCMs' simulation of temperature variations for any hope of non-local effects to be faithfully reproduced. Therefore, an assessment of the local response would elucidate to what extent the GCMs' non-local snow responses aid or hinder overall simulation skill.

i) Snow cover and the surface energy budget

To identify regions in which the prescribed snow conditions would most likely invoke a considerable local atmospheric response, consider a generalized depiction of the surface energy budget:

$$C\frac{dT_s}{dt} = (1-\alpha)SW + LW_d - LW_u - LH - SH - G - M \qquad (1)$$

where T_s is the surface temperature, C is the thermal inertia of the soil surface, " is the surface albedo, SW is the incident shortwave radiation, LW_d is the incident longwave radiation, LW_u is the upward longwave radiation, LH is the latent heat flux, SH is the sensible heat flux, G is the ground heat flux and M is the energy flux required to melt snow. During springtime conditions, the most considerable impact of a change in snow conditions from the prescribed snow in the SASE numerical experiments is to change the surface albedo. This will then modify the amount of solar energy absorbed/reflected at the surface and, in turn, modify fluctuations in the surface temperature, and given its close proximity, will also affect T_a. Therefore, from a "local" (*i.e.*, grid-point) perspective, our assessment of the impacts of the prescribed snow conditions in the SASE experiments will begin with looking at changes in snow and how they would affect the first term on the right-hand side of (1).

In both the COLA and GEOS GCMs, the land modules modify the aggregate grid-box albedo according to the fractional coverage of snow. For the COLA GCM, snow cover is

a diagnostic variable that is linearly and exclusively dependent on the snow water equivalent depth (SWE). The fractional cover of snow, F_S, over a grid-box is assumed to increase linearly, starting at 0% at a value of SWE=0 mm and achieves 100% coverage at a value of SWE=10 mm. The aggregate grid-box albedo, $"_G$, is modified by the combined effects of snow albedo, $"_S$, (which is constant in time) and the underlying albedo of the vegetation/soil, $"_V$, by the following expression:

$$\alpha_G = (1 - F_S)\alpha_V + F_S\alpha_S \tag{2}$$

Therefore, changes in the fractional cover of snow at a grid-box translate linearly into changes in the aggregate grid-box albedo. The fractional snow cover relation in the HY-SSiB land-surface model in the GEOS AGCM is a function of the liquid equivalent snow depth and snow density (which varies in time) in the grid square. This function was designed to slowly increase the fractional snow with depth, then to increase more rapidly before asymptotically approaching 1.0. The slope of this function is dependent on the snow density, with denser (less dense) snow resulting in a lower (higher) snow fraction given the same snow depth. Freshly fallen snow tends to be less dense, but would have higher snow coverage, whereas older denser snow may have melted in various areas, leading to a decrease in the fractional amount. Further details on this relation can be found in Mocko and Sud (2001, Eqs. 3-5 and Fig. 3).

Variations in albedo, due to changes in snow cover, will only affect (1) to any notable degree when an ample supply of *SW* also exists (and thus the amount of absorbed solar

insolation would be subsequently modulated). In the context of the seasonal simulations conducted, a simple measure to characterize the coincidence of these conditions would be:

$$\sigma_{SC}\overline{SW} \equiv A_S \tag{3}$$

where σ_{SC} is the standard deviation of monthly mean fractional snow cover and $\overline{SW}$ is the monthly mean incident shortwave radiation at the surface. By this measure, regions of relatively high values of A_S would denote that the potential of a **local impact** from the "assimilated" snow is also high, and therefore, we would expect the most notable changes in T_a (and potential increases in T_a skill) to occur as a result of the prescribed snow conditions.

Both the COLA and GEOS GCMs show a fair degree of consistency in the springtime progression of A_S (Fig. 9). Generally speaking, the global patterns of A_S follow a northerly retreat (as one might expect) in both GCMs during the March-June simulation period (Fig. 9 shows the patterns for March-May). In March, the strongest regions of A_S occur along the US-Canada border in North America, over the Alps and Baltic regions in western Eurasia, over the Himalayas and along the 50E N latitude line across eastern Asia. In April, both models show the strongest A_S regions located within a large portion of Canada, Russia and the Baltic countries, and considerable values of A_S remain over the major Northern Hemisphere mountainous regions (i.e. Rockies, Alps and Himalayas). By May, most of the strongest A_S areas in both models are confined to the northernmost

regions of Russia (though the COLA maxima is slightly south of GOES') and Canada. For the most part, the COLA GCM's values of A_S are stronger in March, and cover a larger area in April (as compared to GEOS GCM), while in May, the GEOS model has higher values of A_S in the far northern regions (with stronger values by the COLA model persisting the Himalayas). Overall, the differences between the COLA and GEOS models' patterns of A_S qualitatively follow those seen for snow cover variability (Fig. 6), and would therefore suggest that differences in the simulation of mean incident solar radiation at the surface play a secondary role.

ii) Localized corrections in simulated temperature anomalies from prescribed snow

In the context of the prescribed – and presumably "corrected" – snow cover conditions of the SASE experiments, localized improvements in the simulation of T_a will not necessarily result in all regions of high A_S. From the discussion regarding the surface energy budget in the preceding section, regions where A_S are high would only be expected to see a locally improved T_a skill in the SASE simulations where the errors in water equivalent snow depth, g_S, and near-surface air temperature, g_T, in the OBOE simulations are of opposite sign. That is, only where snow errors in the OBOE simulations exist, and are removed in the SASE simulations, will any effect on the surface energy budget occur. The subsequent change in temperature will most likely be opposite in sign (given a coincident and sufficiently high A_S) to that of the prescribed change in the snow conditions. Therefore, to determine the extent of these local impacts in the SASE simulations, the anomaly correlation and RMS diagnostics were repeated,

but only for land points in which A_S was above a minimal threshold value (=5 W/m^2) and where the following condition was met for the monthly mean snow and T_a errors in the OBOE simulations:

$$\varepsilon_S \varepsilon_T \leq -0.25. \tag{4}$$

In determining the product term in (4), each of the error terms, ε_S and ε_T, was normalized against the standard deviation of simulated monthly mean water equivalent snow depth and T_a respectively. Therefore the product term on the left-hand side of (4) is unitless. Thus, the conditional placed on the error product corresponds to when/where the two error terms must be of opposite sign, and the magnitude of both the errors is at least a half a standard deviation unit (or equivalently so as a result of their product). The minimum threshold value of A_S was chosen by noting that this metric loosely reflects an average amount of incident solar energy that coincides with snow cover variability. If 5 W/m^2 of surface energy flux was used exclusively for melting snow over the course of a month, it would melt ~40 mm of water equivalent depth of a snow pack. Given our assumed constant snow density of 200 kg/m^3 (or a 5:1 snow depth to water equivalent depth ratio), this translates into an actual (i.e. not water equivalent) snow depth of ~200mm, which is a typical value of the snow pack conditions on April 1, based on the USAF analysis (Fig. 1).

Upon recalculation of the correlation and RMS diagnostics (Figs. 10 and 11), a substantially more ubiquitous improvement in T_a skill is seen for both of the models

(compared to Figs. 7 and 8). On average, both the models see a reduction in RMS error of about 0.25K and an increase in spatial correlation of about 0.3 (though the largest increases are 0.8 for COLA and 1.4 for GEOS). The changes in RMS error and correlation between the SASE and OBOE simulations for the GEOS GCM are somewhat more variable from year to year (as compared to the COLA GCM), and could be a result of the GEOS experiments being conducted with only single runs (as opposed to the COLA GCM's 10 member ensembles). What is perhaps interesting to note is that for the COLA model, the largest improvements to the correlation skill scores occur in non-ENSO years (denoted by red and blue shaded years); however, the GEOS model shows no such exclusionary features to its correlation response (*i.e.*, one of the largest improvements in the anomaly correlation occurs in the El Niño of 1982/83).

4. Concluding Remarks

Based on a suite of seasonal simulations (March-June) spanning the years 1982-1998 conducted by the COLA and GEOS GCMs, the prescription of "realistic" snow conditions is found to impose a discernable "local" impact on the skill of near-surface air temperature skill. However, the overall results indicate that the impact of the prescribed snow conditions on skill is not robust. This therefore suggests that the GCMs not only have difficulty in depicting the degree to which local skillful responses translate into non-local impacts, but in some cases the non-local response is unskillful (and thus offsets the local, skillful response). The results also indicate that the most notable impact of the

prescribed snow conditions occurs during April, when the retreat of the ephemeral Northern Hemisphere snow cover is typically at its greatest.

Several caveats, from the construction of these experimental simulations to the subsequent analyses, must be considered. The assignment of the globally constant value of snow density (to convert the USAF snow depth data to a water-equivalent value) is certainly not what occurs in nature. Therefore, inaccuracies in this globally constant assignment of snow density would lead to inaccuracies in the prescribed snow conditions, and would lead to inaccurate temperature responses from the GCMs. In addition, errors in the USAF snow depths (previously discussed) and in the CAMS temperature fields can also affect the comparisons of the results between the models, between the two experiment sets, and between the various years. Since the implementation of the USAF snow conditions is likely to be imperfect, our assessment of the snow "correction" impact on the GCMs temperature skill is then an underestimate. This analysis also presents results from only two GCMs, and the quantitative assessments of the snow-climate sensitivities are likely to be considerably model dependent.

The differences between the COLA and GEOS GCMs in the response to the prescribed snow conditions could be affected by a number of reasons (i.e. differences in the numerical representation of precipitation, cloud processes, radiation, land processes, etc.). However, it is important to note that for the GEOS model, the SASE experiments were not performed to an ensemble of simulations, and reflect only the response of the snow conditions from one simulation. Therefore, a certain degree of noise is probable in the

diagnostics of these experiments. It is not unreasonable to expect that upon constructing ensembles of both the OBOE and SASE experiments that an increase in the ubiquity in the T_a skill response would result (and the apparent "negative" skill responses of 1986 and 1994 would be reversed). Unfortunately, due to computational limitations, the extension of the single-run GEOS simulations to ensembles was not possible.

Nevertheless, the notable improvement of T_a skill – on a local basis – from both of the GCMs is encouraging. The results would imply, however, that the non-local/remote response to the prescribed snow conditions is questionable. These shortcomings are likely caused by a complex interaction of atmospheric dynamics, physics, and land-atmosphere coupling within a GCM. However, the ability of a climate model to faithfully execute non-local responses to snow variations would fundamentally rest upon the accurate translation/advection of local, near-surface atmospheric responses. This would therefore demand atmospheric boundary layer processes, which are parameterized in most GCMs for computational efficiency, be more explicitly represented in GCMs so that a near-surface response is more accurately advected into the "free atmosphere". Subsequently, the numerical representation of cloud, radiative, dynamical and precipitation processes would all play a critical role in the accurate depiction of snow-climate teleconnections. Holistically speaking, all physical parameterizations in GCMs must be improved before all prediction enhancements from improved snow simulations can be realized.

5. Acknowledgements

The authors wish to thank Paul Dirmeyer and Jagadish Shukla for their support and use of the COLA AGCM in these experiments, as well as Y. C. Sud for his development and insight into the GEOS GCM. The authors are also grateful for the efforts of Mike Fennessy (COLA) in processing and preparing the USAF snow data. Figs 1-6 and 9 were created with the GrADS software package created by Brian Doty. The authors also wish to thank the three anonymous reviewers, whose comments lead to a substantially improved paper.

References

Bamzai, A. S., and J. Shukla, 1999: Relation between Eurasian snow cover, snow depth, and the Indian summer monsoon: an observational study. *J. Climate*, **12**(10), 3117-3132.

Chou, M.-D., and M. J. Suarez, 1994: An efficient thermal infrared radiation parameterization for use in general circulation models. *NASA Tech. Memo. 104606*, *Vol. 3*. Goddard Space Flight Center, Greenbelt MD 20771, 102 pp.

Chou, M.-D., K.-T. Lee, S.-C. Tsay, and Q. Fu, 1999: Parameterization of cloud longwave scattering for use in atmospheric models. *J. Climate*, **12**(1), 159-169.

Chou, M.-D., M. J. Suarez, C.-H. Ho, M.-H. Yan, and K.-T. Lee, 1998: Parameterizations for cloud overlapping and shortwave single scattering properties for use in general circulation and cloud ensemble models. *J. Climate*, **11**(2), 202-214.

Cohen, J., and D. Rind: 1991: The effect of snow cover on the climate. *J. Climate*, **4**(7), 689-706.

Conaty, A. L., J. C. Jusem, L. Takacs, D. Keyser, and R. Atlas, 2001: The structure and evolution of extratropical cyclones, fronts, jet streams, and the tropopause in the GEOS general circulation model. *Bull. Amer. Meteor. Soc.*, **82**(9), 1853-1867.

Dirmeyer, P. A., A. J. Dolman, and N. Sato, 1999: The pilot phase of the Global Soil Wetness Project. *Bull. Amer. Meteor. Soc.*, **80**(5), 851-878.

Dirmeyer, P. A., and F. J. Zeng, 1999: An update to the distribution and treatment of vegetation and soil properties in SSiB. *COLA Technical Report 78* [Available

from the Center for Ocean Land Atmosphere Studies, 4041 Powder Mill Road, Suite 302, Calverton, MD 20705 USA] 25 pp.

Dirmeyer, P. A., and L. Tan, 2001: A multi-decadal global land-surface data set of state variables and fluxes. *COLA Technical Report 102* [Available from the Center for Ocean Land Atmosphere Studies, 4041 Powder Mill Road, Suite 302, Calverton, MD 20705 USA] 25 pp.

Doesken, N. J., and A. Judson, 1997: *The Snow Booklet: A Guide to the Science, Climatology, and Measurement of Snow in the United States*. [Available from Colorado State University, Dept. of Atmospheric Sciences, Ft. Collins, CO 80523 USA] 87 pp.

Fennessy, M., and C. A. Schlosser, 2002: A 46 km x 46 km daily, global snow analysis suitable for climate studies. *COLA Technical Report*, submitted.

Foster, Jr., D. J., and R. D. Davey, 1988: Global snow depth climatology, OL-A, USAFETAC, Asheville, NC, *USAFETAC/TN-88/006*.

Foster, J., G. Liston, R. Koster, R. Essery, H. Behr, L. Dumenil, D. Verseghy, S. Thompson, D. Pollard, and J. Cohen, 1996: Snow cover and snow mass intercomparisons of general circulation models and remotely sensed datasets. *J. Climate*, **9**(2), 409-426.

Foster, J., M. Owe, and A. Rango, 1983: Snow cover and temperature relationships in North American and Eurasia. *J. Appl. Meteor.*, **22**(3), 460-469.

Groisman, P. Ya., T. R. Karl, and R. W. Knight, 1994: Observed impact of snow cover on the heat balance and the rise of continental spring temperatures. *Science*, **263**(5144), 198-200.

Hall, S. J., 1986: AFGWC Snow analysis model, United States Air Force, *AFGWC/TN-86/001*.

Helfand, M. H., and J. C. Lebraga, 1988: Design of a non-singular level 2.5 second-order closure model for prediction of atmospheric turbulence. *J. Atmos. Sci*., **45**(2), 113-132.

Kalnay, E., M. Kanamitsu, R. Kistler, W. Collins, D. Deaven, L. Gandin, M. Iredell, S. Saha, G. White, J. Woollen, Y. Zhu, M. Chelliah, W. Ebisuzaki, W. Higgins, J. Janowiak, K. C. Mo, C. Ropelewski, J. Wang, A. Leetmaa, R. Reynolds, R. Jenne, and D. Joseph, 1996: The NCEP/NCAR 40-year reanalysis project. *Bull. Amer. Meteor. Soc.*, **77**(3), 437-471.

Kinter, J. L. III, D. Dewitt, P. A. Dirmeyer, M. J. Fennessy, B. P. Kirtman, L. Marx, E. K. Schneider, J. Shukla, and D. M. Straus, 1997: The COLA atmosphere-biosphere general circulation model volume 1: Formulation. *COLA Technical Report 51* [Available from the Center for Ocean Land Atmosphere Studies, 4041 Powder Mill Road, Suite 302, Calverton, MD 20705 USA] 43 pp.

Mocko, D. M., and Y. C. Sud, 2001: Refinements to SSiB with an emphasis on snow-physics: Evaluation and validation using GSWP and Valdai Data. *Earth Interactions*, **5**(5-001), 31 pp.

Mocko, D. M., Y. C. Sud, and G. K. Walker, 1999: New snow-physics to complement SSiB. Part II: Effects on soil moisture initialization and simulated surface fluxes, precipitation and hydrology of GEOS II GCM. *J. Meteor. Soc. Japan*, **77**(1B), 335-348.

Namias, J., 1985: Some empirical evidence for the influence of snow cover on temperature and precipitation. *Mon. Wea. Rev.*, **113**(9), 1542-1553.

Posey, J. W. and P. F. Clapp, 1954: Global distribution of normal surface albedo. *Geofisica Int.*, **4**, 33-48.

Ropelewski, C. F., J. E. Janowiak, and M. S. Halpert, 1985: The analysis and display of real time surface climate data. *Mon. Wea. Rev.*, **113**(6), 1101-1106.

Schlosser, C. A., and P. A. Dirmeyer, 2000: Climate variability and potential predictability over continental regions in response to SST variations. *COLA Technical Report 91* [Available from the Center for Ocean Land Atmosphere Studies, 4041 Powder Mill Road, Suite 302, Calverton, MD 20705 USA] 42 pp.

Schlosser, C. A., A. G. Slater, A. Robock, A. J. Pitman, K. Ya. Vinnikov, A. Henderson-Sellers, N. A. Speranskaya, K. Mitchell, and the PILPS 2(d) Contributors, 2000: Simulations of a boreal grassland hydrology at Valdai, Russia: PILPS Phase 2(d). *Mon. Wea. Rev.*, **128**(2), 301-321.

Schneider, E. K., 2002: Understanding differences between the equatorial Pacific as simulated by two coupled GCMs. *J. Climate*, **15**(5), 449-469.

Sela, J. G., 1980: Spectral modeling at the National Meteorological Center. *Mon. Wea. Rev.*, **108**(9), 1279-1292.

Shukla, J., J. Anderson, D. Baumhefner, C. Brankovic, Y. Chang, E. Kalnay, L. Marx, T. Palmer, D. Paolino, J. Ploshay, S. Schubert, D. Straus, M. Suarez, and J. Tribbia, 2000: Dynamical Seasonal Prediction. *Bull. Amer. Meteor. Soc.*, **81**(11), 2593-2606.

Slater, A. J., C. A. Schlosser, C. E. Desborough, A. J. Pitman, A. Henderson-Sellers, A. Robock, K Ya. Vinnikov, K. Mitchell, and the PILPS 2(d) Contributors, 2001: The representation of snow in land-surface schemes: Results from PILPS 2(d). *J. Hydromet.*, **2**(1), 7-25.

Sud, Y. C., and D. M. Mocko, 1999: New Snow-Physics to Complement SSiB. Part I: Design and evaluation with ISLSCP Initiative 1 Datasets. *J. Meteor. Soc. Japan*, **77**(1B), 335-348.

Sud, Y. C., and G. K. Walker, 1999a: Microphysics of Clouds with the relaxed Arakawa-Schubert Scheme (McRAS). Part I: Design and evaluation with GATE Phase III data. *J. Atmos. Sci.*, **56**(18), 3196-3220.

Sud, Y. C., and G. K. Walker, 1999b: Microphysics of Clouds with the relaxed Arakawa-Schubert Scheme (McRAS). Part II: Implementation and performance in GEOS 2 GCM. *J. Atmos. Sci.,* **56**(18), 3121-3240.

Sud, Y. C., D. M. Mocko, K.-M. Lau, and R. Atlas, 2002: On simulating the Midwestern U.S. drought of 1988 with a GCM. *J. Climate*, submitted.

Takacs, L. L., A. Molod, and T. Weng, 1994: Documentation of the Goddard Earth Observing System (GEOS) General Circulation Model Ver. 1. *NASA Tech. Memo. 104606, Vol. 1.* Goddard Space Flight Center, Greenbelt MD 20771, 100 pp.

Urban, B., 1996: Coherent observation operators for surface data assimilation with application to snow depth. *J. Appl. Meteor.*, **35**(2), 258-270.

Vernekar, A. D., J. Zhou, and J. Shukla, 1995: The effect of Eurasian snow cover on the Indian monsoon. *J. Climate*, **8**(2), 248-266.

Walsh, J. E., and B. Ross, 1988: Sensitivity of 30-day dynamical forecasts to continental

snow cover. *J. Climate*, **1**(7), 739-756.

Warren, S.G., 1984: Impurities in snow: effects on albedo and snowmelt. *Annals of Glaciology*, **5**, 177-179.

Xue, Y., P. J. Sellers, J. L. Kinter III, and J. Shukla, 1991: A Simplified Biosphere model for global climate studies. *J. Climate*, **4**(3), 345-364.

Yang, F., A. Kumar, W. Wang, H.-M. H. Juang, and M. Kanamitsu, 2001: Snow-albedo feedback and seasonal climate variability over North America. *J. Climate*, **14**(22), 4245-4248.

Zhou, J., Y. C. Sud, and K.-M. Lau, 1996: Impact of orographically induced gravity-wave drag in the GLA GCM. *Quart. J. Roy. Meteor. Soc.*, **122**(532), 903-927.

Figure Captions

Figure 1. Averaged snow depth (1979-1998) for the 1st day of the months of March-June based upon the USAF daily snow depth analysis.

Figure 2. Average April snow cover (1982-1998) for the OBOE (top panel) and SASE (middle panel) simulations with the COLA GCM. The difference between the SASE and OBOE simulations is given in the bottom panel. Units are in %. Results shown for the Northern Hemisphere between 20EN and 75EN.

Figure 3. As in Fig. 2, but for simulated near-surface air temperature. Units are in ^{o}C.

Figure 4. As in Fig. 2, but for the GEOS GCM simulations.

Figure 5. As in Fig. 3, but for the GEOS GCM simulated near-surface air temperature.

Figure 6. Standard deviation of April snow cover (%) as simulated by the COLA (left panels) and GEOS (right panels) GCM seasonal simulations (1982-1998). Shown is the simulated snow cover over the Northern Hemisphere between 20EN and 75EN. The top panels are from the OBOE simulations and the middle panels are from the SASE simulations. The differences between the OBOE and SASE simulations are given in the bottom panels.

Figure 7. Spatial correlation coefficients between simulated and observed April near-surface air temperature anomalies for all land points between 20EN and 75EN. The top panel shows the results for the COLA GCM, and the bottom panel shows the results for the GEOS GCM. Observations are based on the CAMS station network. The correlations are performed for all years of the seasonal simulations (1982-1998). In each panel, the correlation results of the OBOE (solid curve) and SASE (dashed curve) simulations are shown. Years in which ENSO conditions occurred are denoted by dark gray (El Niño) and light gray (La Niño) shading.

Figure 8. Root-mean square (RMS) error of simulated April near-surface air temperature by the COLA (top panel) and GEOS (bottom panel) GCMs. RMS errors are calculated for all land points between 20EN and 75EN. Observations are based on the CAMS station network. In each panel, RMS errors from the OBOE (solid curve) and SASE (dashed curve) simulations are given.

Figure 9. Seasonal progression of the product of standard deviation of monthly snow cover and monthly mean incident shortwave radiation, $\sigma_{SC}\overline{SW}$, as simulated by the COLA (left panels) and GEOS (right panels) GCMs. Shown are the results from March thru May (going from top to bottom) over the Northern Hemisphere between 20EN and 75EN. Units are in W/m^2.

Figure 10. Spatial correlation coefficients between simulated and observed April near-surface air temperature anomalies, based on land points between 20EN and 75EN that

contain a high potential for a localized impact from snow assimilation (described in text). The top panel shows the results for the COLA GCM, and the bottom panel shows the results for the GEOS GCM. Observations are based on the CAMS station network. The correlations are performed for all years of the seasonal simulations (1982-1998). In each panel, the correlation results of the OBOE (solid curve) and SASE (dashed curve) simulations are shown.

Figure 11. Root-mean square (RMS) error of simulated April near-surface air temperature by the COLA (top panel) and GEOS (bottom panel) GCMs. RMS errors are calculated for all land points between 20EN and 75EN that contain a high potential for a localized impact from snow assimilation (described in text). Observations are based on the CAMS station network. In each panel, RMS errors from the OBOE (solid curve) and SASE (dashed curve) simulations are given.

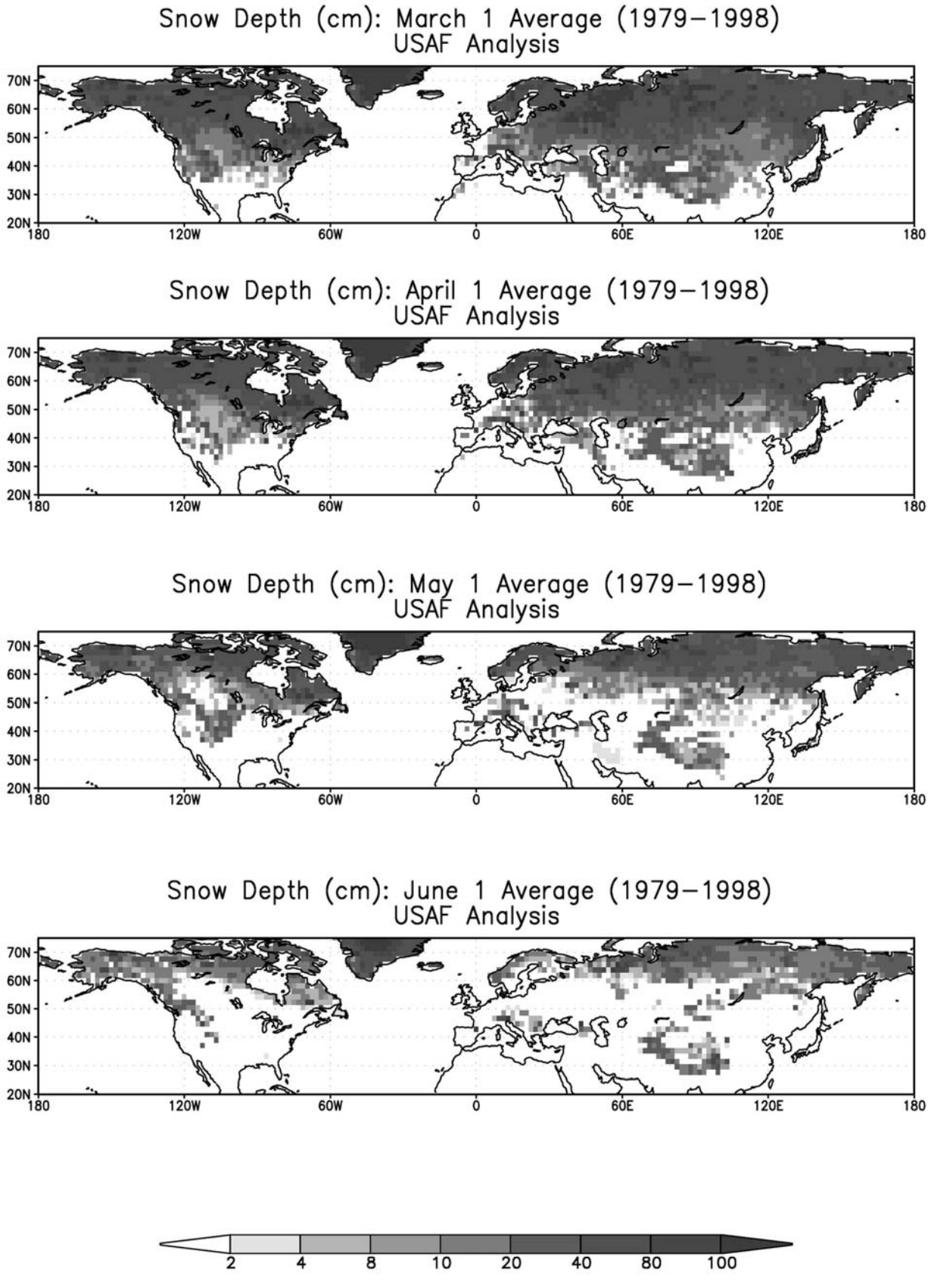
Snow Depth (cm): March 1 Average (1979–1998)
USAF Analysis
Snow Depth (cm): April 1 Average (1979–1998)
USAF Analysis
Snow Depth (cm): May 1 Average (1979–1998)
USAF Analysis
Snow Depth (cm): June 1 Average (1979–1998)
USAF Analysis
70N
60N
50N
40N
30N
20N
180
120W
60W
0
60E
120E
180
2
4
8
10
20
40
80
100

Figure 1

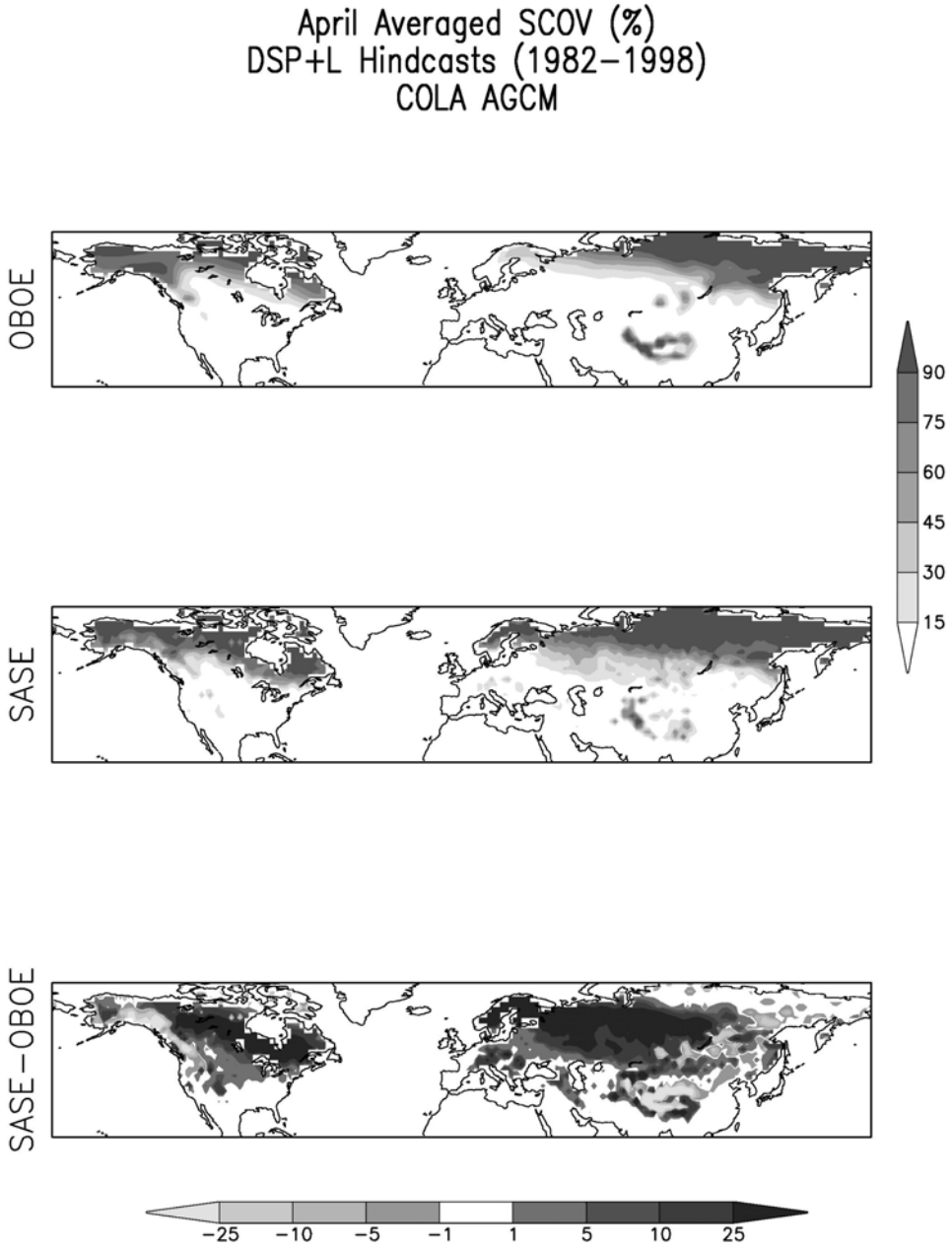
April Averaged SCOV (%)
DSP+L Hindcasts (1982–1998)
COLA AGCM
OBOE
SASE
SASE–OBOE
90
75
60
45
30
15
−25
−10
−5
−1
1
5
10
25

Figure 2

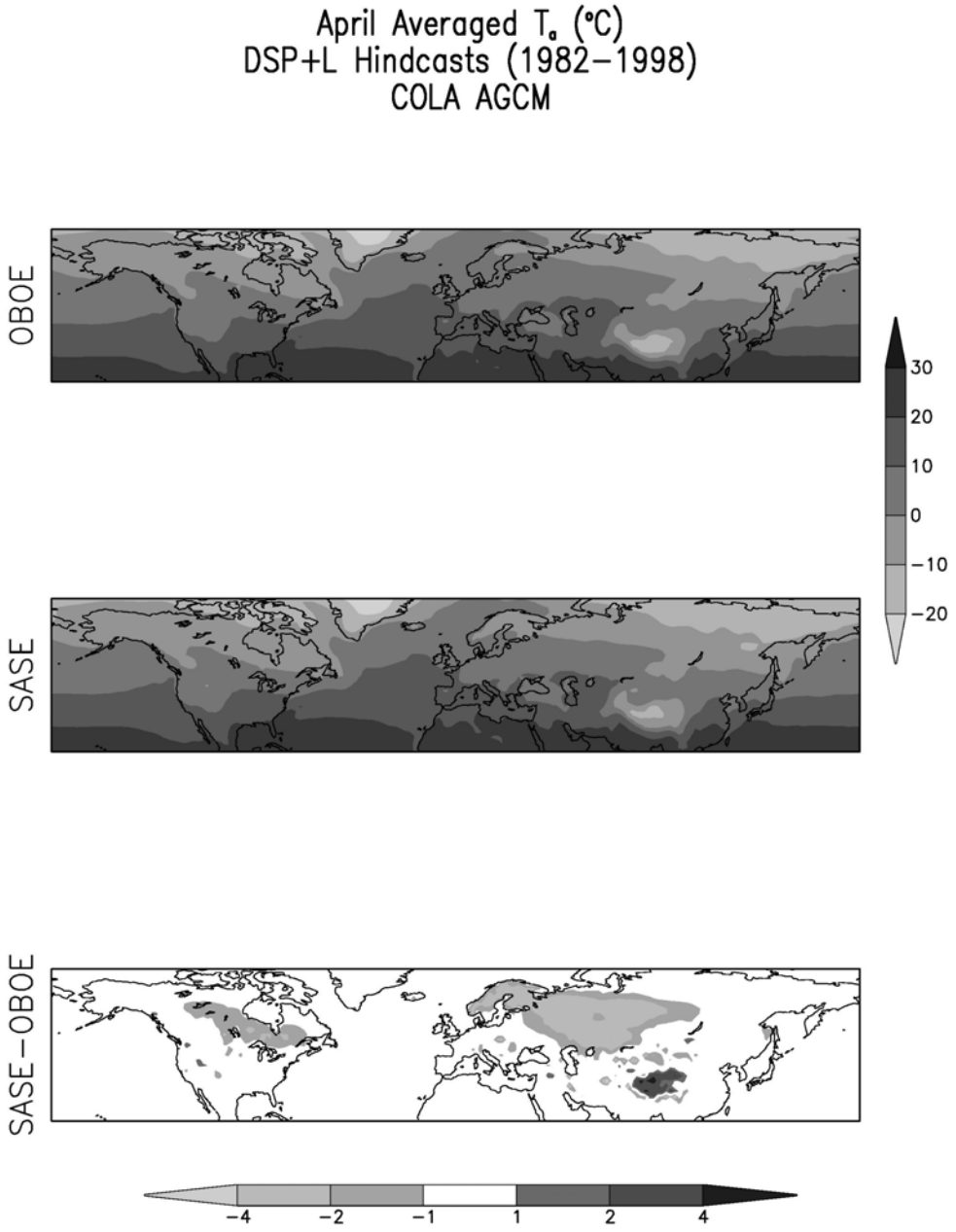
April Averaged T_a (°C)
DSP+L Hindcasts (1982–1998)
COLA AGCM
OBOE
SASE
SASE–OBOE
30
20
10
0
–10
–20
–4
–2
–1
1
2
4

Figure 3

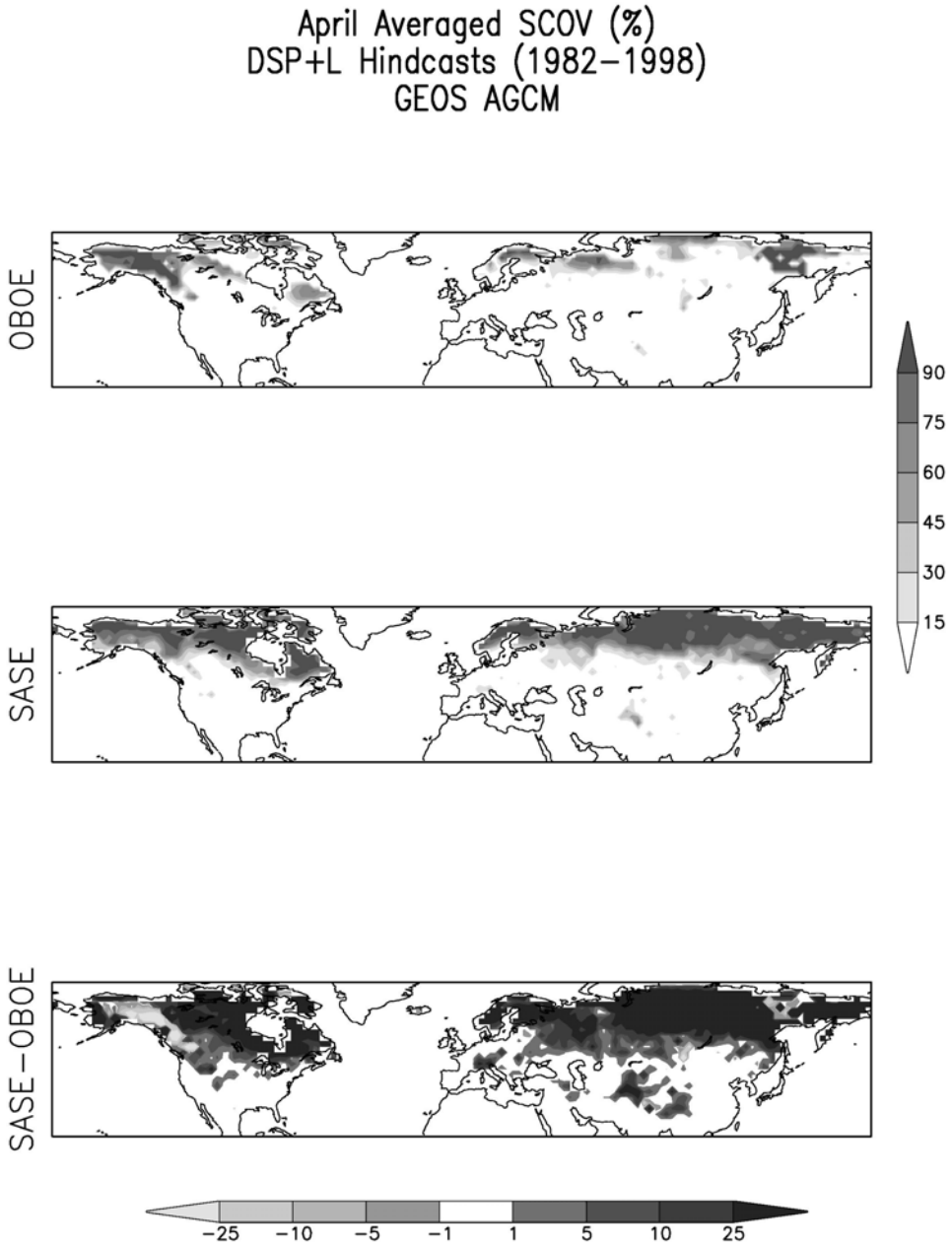
April Averaged SCOV (%)
DSP+L Hindcasts (1982–1998)
GEOS AGCM
OBOE
SASE
SASE–OBOE
90
75
60
45
30
15
−25
−10
−5
−1
1
5
10
25

Figure 4

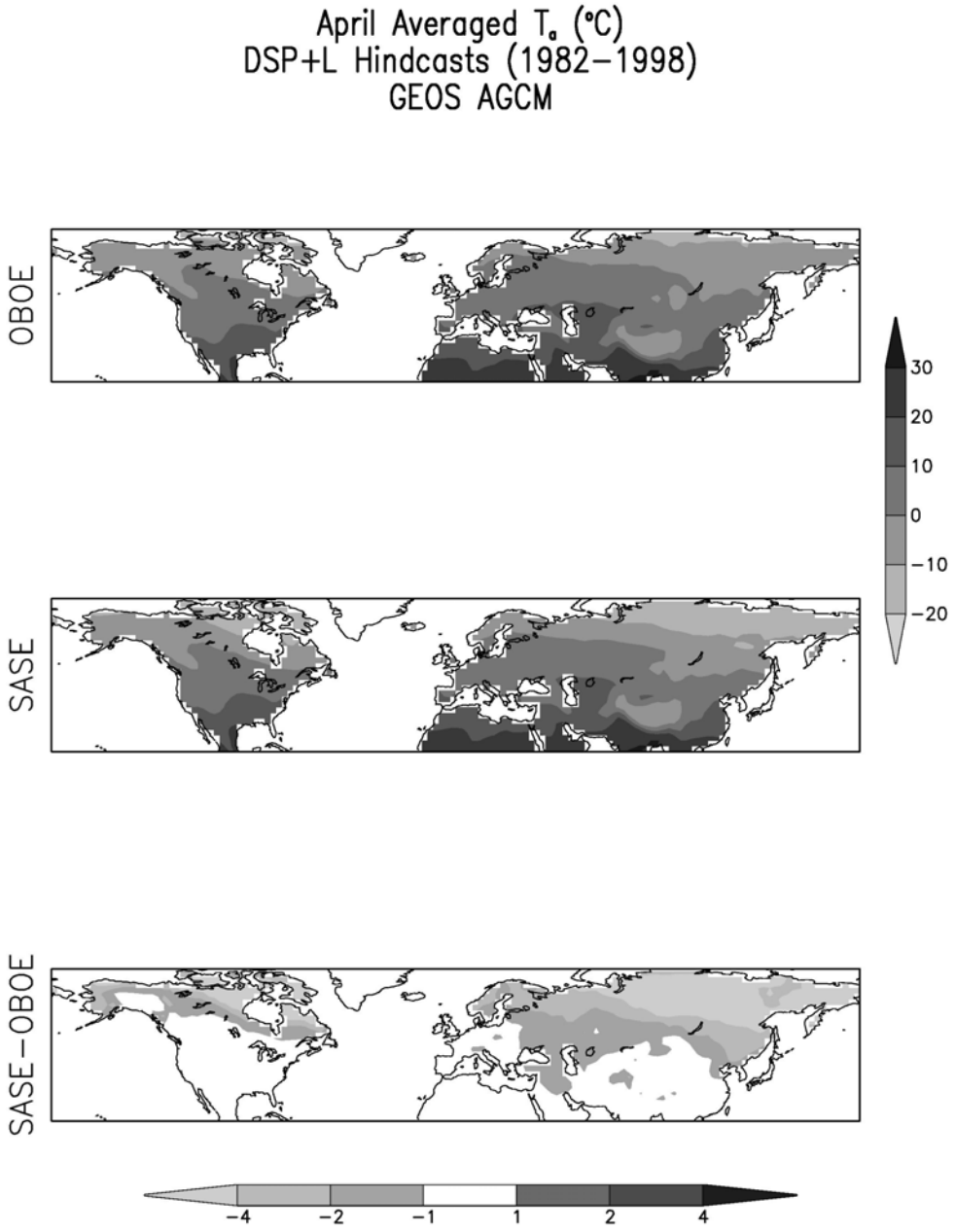
April Averaged T_a (°C)
DSP+L Hindcasts (1982–1998)
GEOS AGCM
OBOE
SASE
SASE–OBOE
30
20
10
0
–10
–20
–4
–2
–1
1
2
4

Figure 5

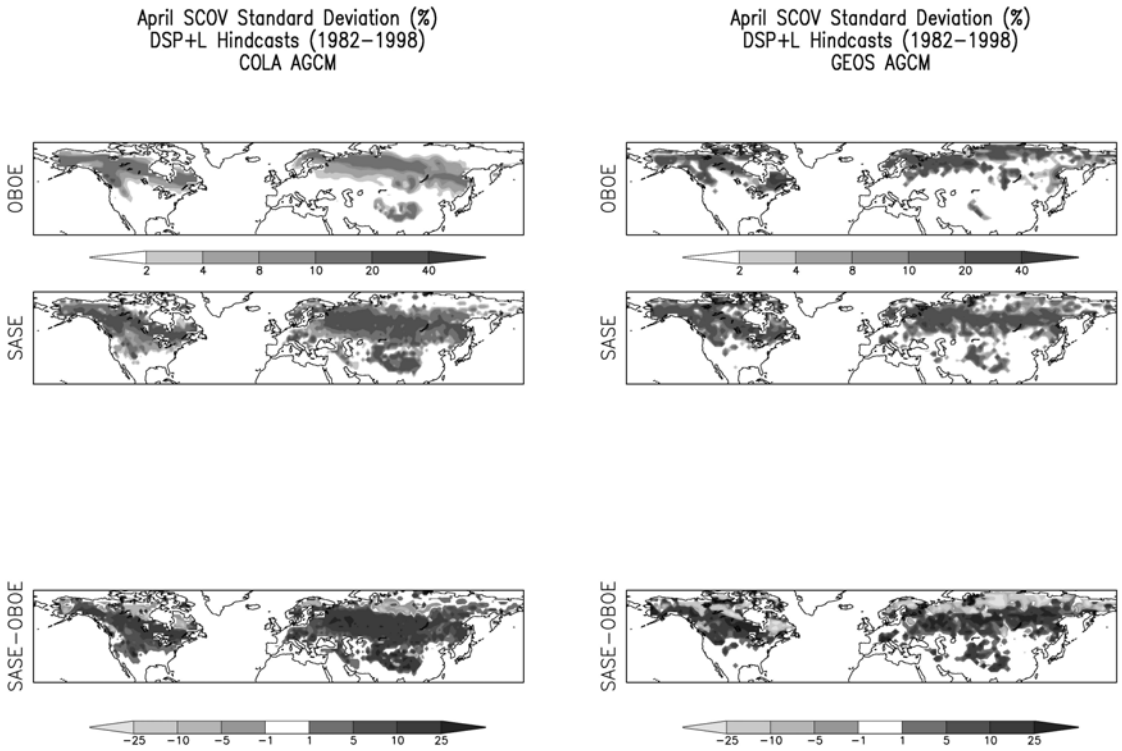
April SCOV Standard Deviation (%)
DSP+L Hindcasts (1982–1998)
COLA AGCM
April SCOV Standard Deviation (%)
DSP+L Hindcasts (1982–1998)
GEOS AGCM
OBOE
SASE
SASE–OBOE
2 4 8 10 20 40
−25 −10 −5 −1 1 5 10 25

Figure 6

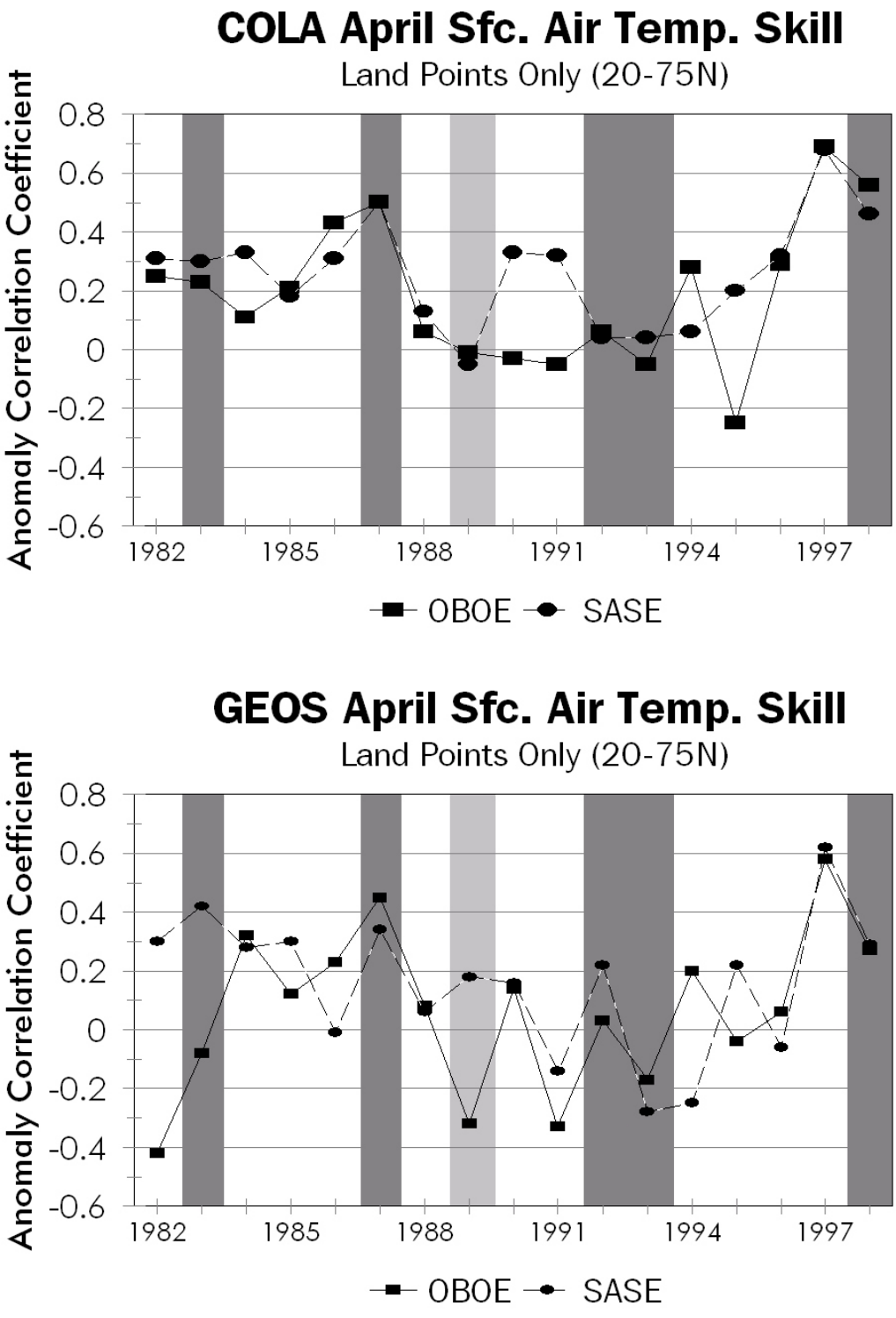
COLA April Sfc. Air Temp. Skill
Land Points Only (20-75N)
Anomaly Correlation Coefficient
0.8
0.6
0.4
0.2
0
-0.2
-0.4
-0.6
1982
1985
1988
1991
1994
1997
OBOE
SASE
GEOS April Sfc. Air Temp. Skill
Land Points Only (20-75N)
Anomaly Correlation Coefficient
0.8
0.6
0.4
0.2
0
-0.2
-0.4
-0.6
1982
1985
1988
1991
1994
1997
OBOE
SASE

Figure 7

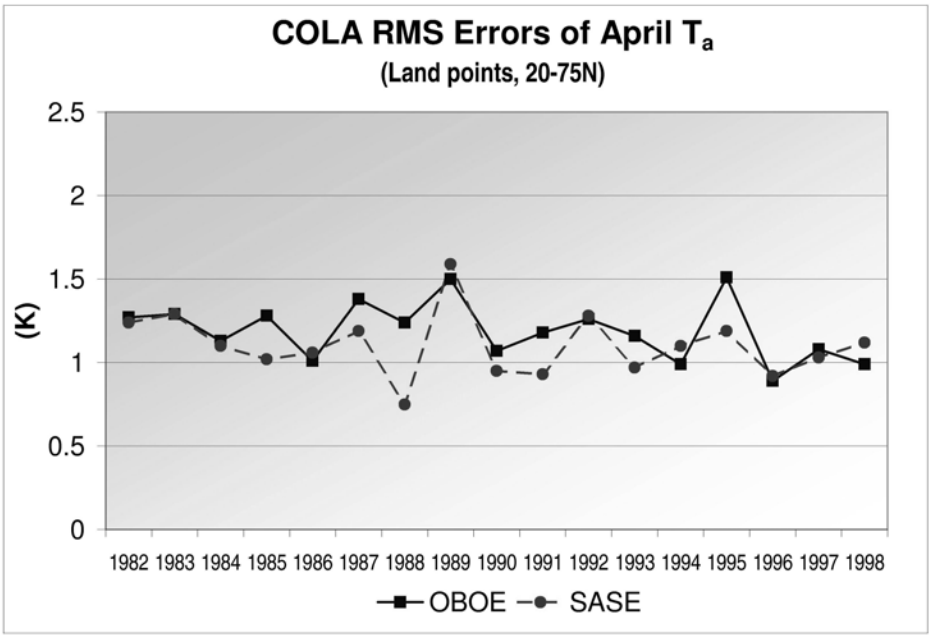
COLA RMS Errors of April T_a
(Land points, 20-75N)
2.5
2
1.5
(K)
1
0.5
0
1982 1983 1984 1985 1986 1987 1988 1989 1990 1991 1992 1993 1994 1995 1996 1997 1998
OBOE
SASE

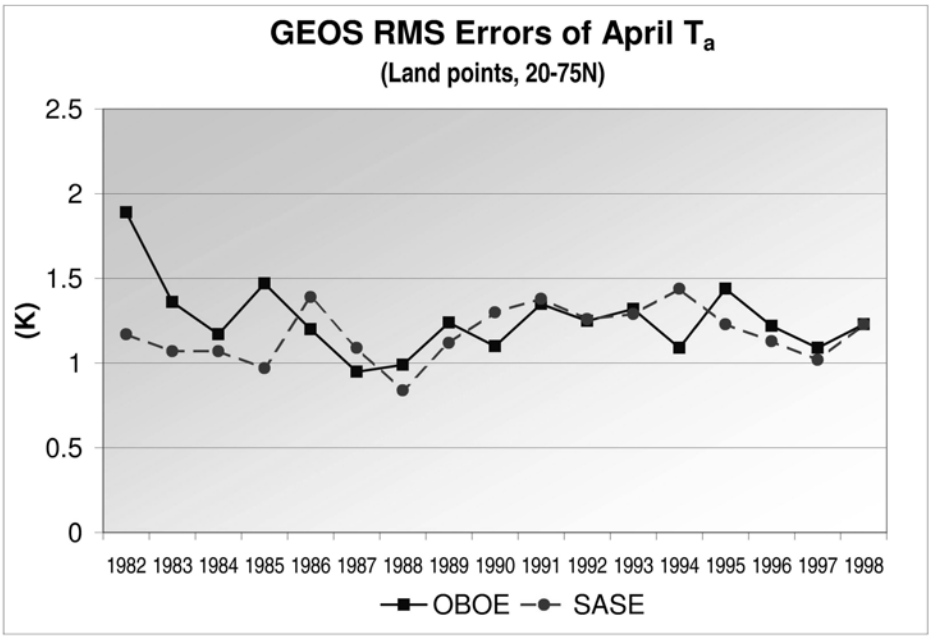
GEOS RMS Errors of April T_a
(Land points, 20-75N)
2.5
2
1.5
(K)
1
0.5
0
1982 1983 1984 1985 1986 1987 1988 1989 1990 1991 1992 1993 1994 1995 1996 1997 1998
OBOE
SASE

Figure 8

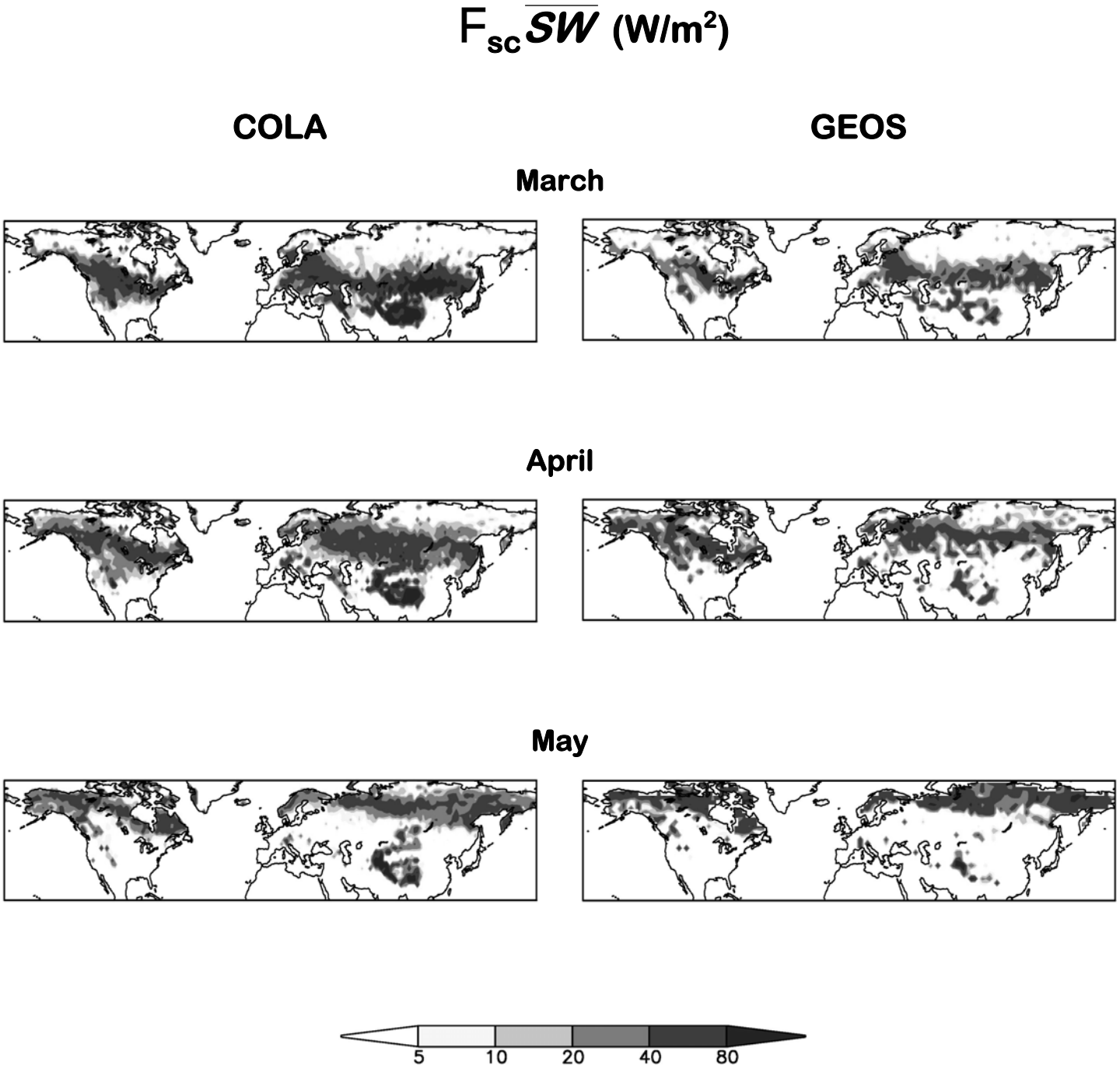

Figure 9

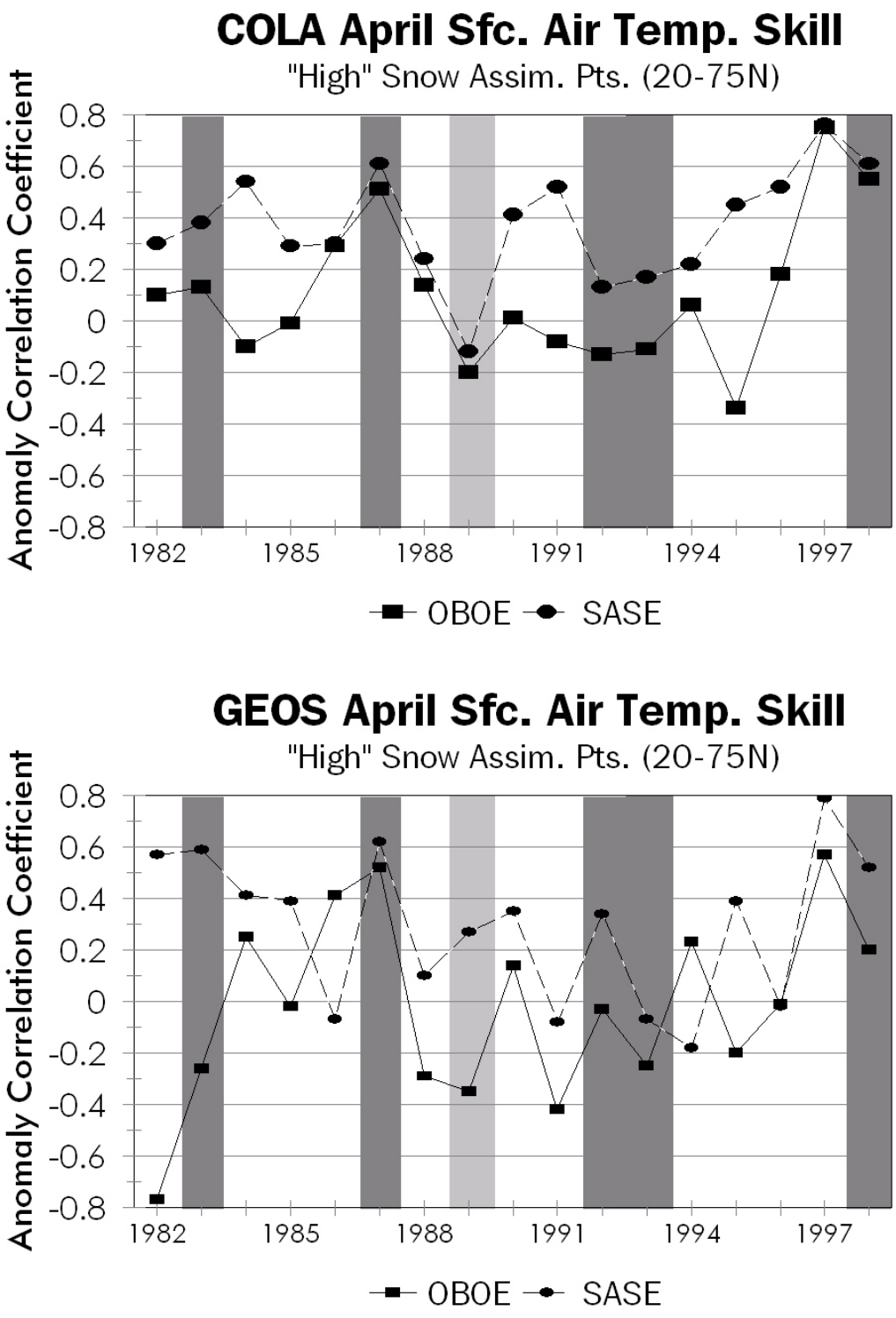
COLA April Sfc. Air Temp. Skill
"High" Snow Assim. Pts. (20-75N)
Anomaly Correlation Coefficient
0.8
0.6
0.4
0.2
0
-0.2
-0.4
-0.6
-0.8
1982
1985
1988
1991
1994
1997
OBOE
SASE
GEOS April Sfc. Air Temp. Skill
"High" Snow Assim. Pts. (20-75N)
Anomaly Correlation Coefficient
0.8
0.6
0.4
0.2
0
-0.2
-0.4
-0.6
-0.8
1982
1985
1988
1991
1994
1997
OBOE
SASE

Figure 10

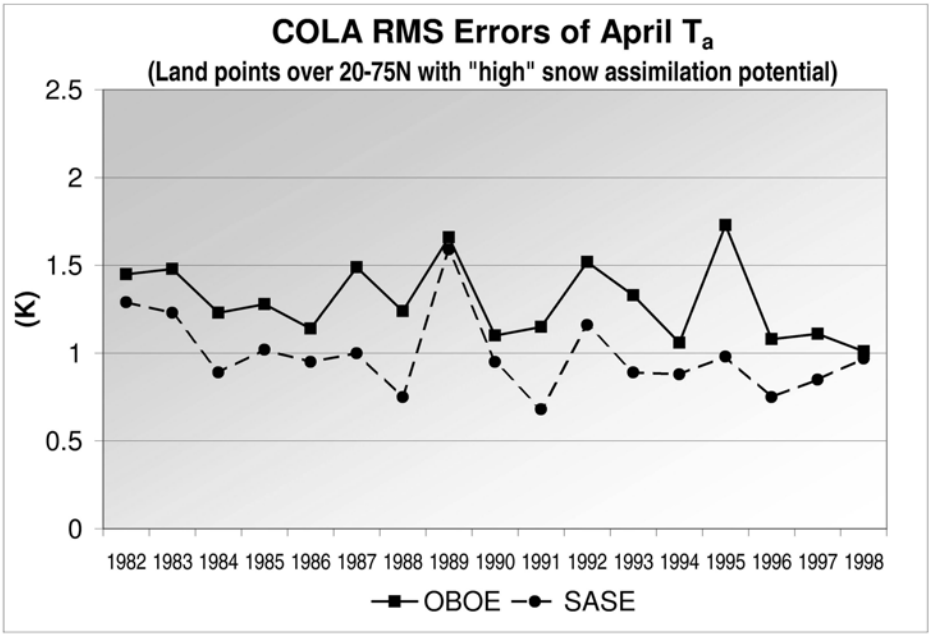
COLA RMS Errors of April T_a
(Land points over 20-75N with "high" snow assimilation potential)
2.5
2
1.5
1
0.5
0
(K)
1982 1983 1984 1985 1986 1987 1988 1989 1990 1991 1992 1993 1994 1995 1996 1997 1998
OBOE
SASE

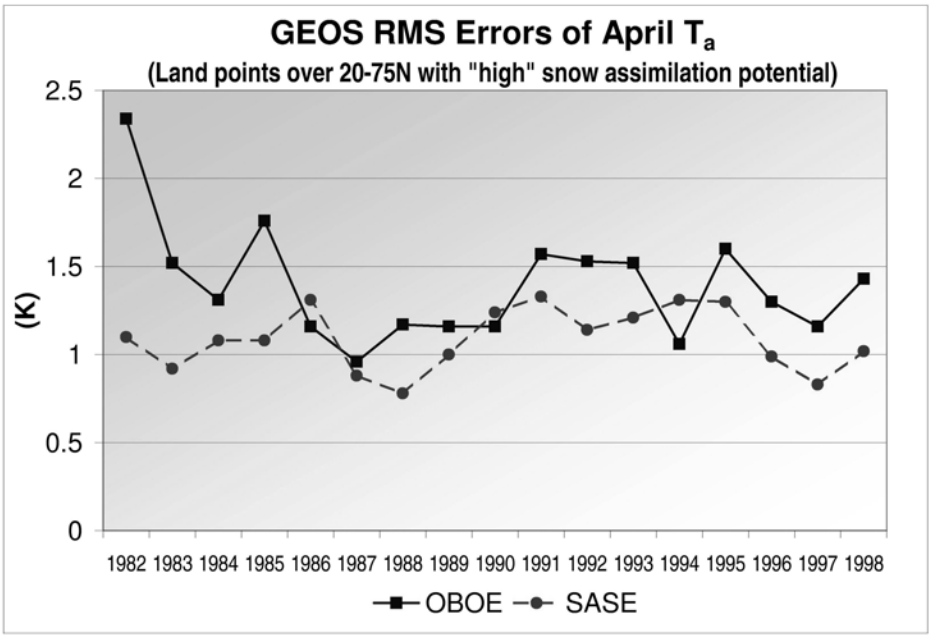
GEOS RMS Errors of April T_a
(Land points over 20-75N with "high" snow assimilation potential)
2.5
2
1.5
1
0.5
0
(K)
1982 1983 1984 1985 1986 1987 1988 1989 1990 1991 1992 1993 1994 1995 1996 1997 1998
OBOE
SASE

Figure 11